

© 2023 Anubhav Bose

SYSTEM-LEVEL OPTIMIZATION OF HIGH-SPECIFIC-POWER
ELECTRIC MACHINES FOR AIRCRAFT PROPULSION
APPLICATIONS

BY

ANUBHAV BOSE

THESIS

Submitted in partial fulfillment of the requirements
for the degree of Master of Science in Electrical and Computer Engineering
in the Graduate College of the
University of Illinois Urbana-Champaign, 2023

Urbana, Illinois

Adviser:

Professor Kiruba Haran

ABSTRACT

High Specific Power and High Efficiency electric machines, particularly in the megawatt class of power, are considered to be key enabling technologies for aircraft electric propulsion. Future aircraft are expected to have a much greater degree of electrification in the propulsion powertrain, which necessitates the development of large electric machines specifically tailored for that purpose. Additionally, weight is at a premium inside an aircraft, which necessitates that the electric powertrain be as light and efficient as possible to maximize the benefits of electrification.

Due to the specialized nature of aerospace propulsion applications, it is imperative that electric machines are specifically designed to fit the particular needs of the specific aircraft. Additionally, the motor needs to integrate seamlessly into the rest of the electric powertrain and the aircraft structure and thermal management systems. Thus, the machine design process needs to account for the considerations derived from these other systems & structures. Developing a motor design & optimization framework that accounts for these considerations is one of the objectives of this thesis work, and the model development, optimization process, and key insights are discussed in the next chapters.

The initial results from this design & optimization process indicate that significant gains in the power density & efficiency of the electric machine can be achieved over the current state-of-the-art, even without changing any assumptions regarding the technology readiness levels or material properties. Additionally, the developed optimization toolset can provide further insight into the different trends of key performance indices of the machines, thus helping the designer understand how these improvements are being achieved.

*To my Parents, for their love, kindness and trust.
And to my friends, for their encouragement, insight and support.*

ACKNOWLEDGMENTS

Above all, I would like to thank my advisor, Professor Kiruba Haran, for his constant support throughout my graduate studies. His mentorship, guidance, insight and support have made my graduate study here in Illinois both successful and enjoyable. I could not have asked for a better advisor to guide me through the ups and downs of graduate school.

I would also like to thank my parents for believing in me, that I could succeed in what I wanted to do, halfway across the world, away from home. Thank you for trusting me, when I set out to pursue my dreams all by myself. And thank you for being with me whenever I needed you the most.

Thank you to the Power and Energy Group here at Illinois. Without you all, I would not have been able to make it this far. The Power Group now holds a special place in my heart, and to me, you are all more than just friends, you are all family. Special thanks go out to Samira Tungare, Elie Libbos, T.G. Roberts, Anjana Samarakoon, Shivang Agrawal, Samith Sirimanna, Max Lewis and Iven Guzel, for being there to pick me up whenever I was down. Thank you so much, it means the world to me.

My gratitude to the Haran Research Group, who have taught me nearly all I know now about Electric Machinery. Thanks to Samith Sirimanna, Xiaolong Zhang and Thanatheepan Balachandran for spending countless hours discussing and helping me with research. I could not have done this without you all. The insights presented in this thesis are not just mine, but yours as well.

Thank you to the staff in the Power and Energy area, Joyce Mast, Kevin Colravy and Robin Smith. Thank you for all your support during PECE, EOH, and everywhere else. This place will not be the same without you all.

Thank you to all my collaborators in the FUTPRINT50 Consortium. The many discussions, meetings and brainstorming events around the project were the foundation behind the motivation of this research. Thank you for

supporting and funding this research, and for helping to bring the vision of electrified aircraft closer to reality.

And last but not the least, a big thank you to all my former teammates at Orion Racing India. The three years I spent there were some of the most fulfilling and intense years of my life. You all taught me the value of dedication, team spirit and having pride in my work. And most importantly, thank you for always putting the team before the car.

TABLE OF CONTENTS

LIST OF TABLES	vii
LIST OF FIGURES	viii
CHAPTER 1 INTRODUCTION	1
1.1 Background	1
1.2 Motivation	2
1.3 Organization of this Thesis	3
CHAPTER 2 MODELLING AND OPTIMIZATION	4
2.1 Machine Structure	4
2.2 Electromagnetics & Loss Mechanisms	5
2.3 Winding & Insulation Design	7
2.4 Heatsink Design	9
2.5 Structural Components & Gearbox Considerations	10
2.6 Mission Profile	10
2.7 Optimization Process	11
CHAPTER 3 DESIGN SPACE EXPLORATION STUDY	13
3.1 Trend Analysis & Pareto Fronts	14
CHAPTER 4 KEY INSIGHTS & DISCUSSION	20
4.1 Comparison Pareto Fronts	20
4.2 Mission Profile Analysis	24
4.3 Improvements from Prior Efforts	26
4.4 On increasing Specific Power and Efficiency	28
CHAPTER 5 CONCLUSION	31
5.1 Key Shortcomings & Challenges	31
5.2 Future Work	33
REFERENCES	35

LIST OF TABLES

4.1	Weight Breakdown Comparison	27
4.2	Comparison of Key Motor Performance Parameters	27

LIST OF FIGURES

1.1	NASA Electric Motor Roadmap for Hybrid-Electric Propulsion [1]	1
2.1	Structure of the High-Specific Power Slotless Motor	5
2.2	Winding Insulation Model Diagram	7
2.3	Heatsink Cross Section	8
3.1	Comparison of Motor Pareto Fronts at different power levels .	17
3.2	Comparison of Motor Pareto Fronts at different voltage levels	18
3.3	Comparison of Motor Pareto Fronts at different RPM cases . .	19
4.1	Voltage Comparison	21
4.2	Direct Drive vs High Speed Reduction Drive	22
4.3	Efficiency Map for an example machine design	25
4.4	Pareto Front of Total Energy Loss in the Mission	25
4.5	Comparison between results of [2] and this thesis	26

CHAPTER 1

INTRODUCTION

1.1 Background

High Power Density Electric machines are a key enabling technology for aircraft electric propulsion [3][4][5]. NASA roadmaps [1] indicate that non-cryogenic conventional electric machines would need to achieve a power density of 19.7 KW/kg (12 hp/lb) by 2030 to enable regional hybrid electric aviation, which is a large increase from the current state-of-the-art at approximately 13.2 KW/kg (8 hp/lb) [6]. This is a clear indication that future electric machines would need highly optimized designs specifically tailored for aircraft propulsion to meet these ambitious goals.

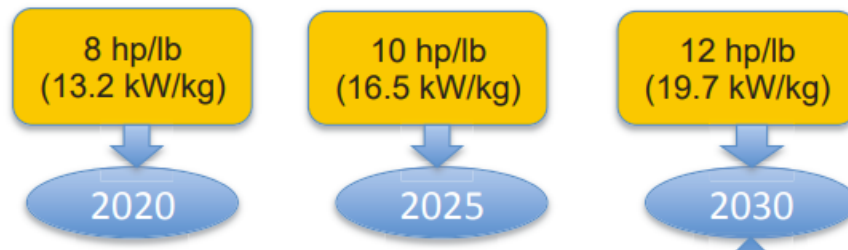


Figure 1.1: NASA Electric Motor Roadmap for Hybrid-Electric Propulsion [1]

Traditionally, in the electric machine design process, only the electromagnetic sizing is performed [7][8][9], with more recent approaches coupling the electromagnetic and thermal analyses together [2]. Addition of thermal analysis in a multiphysics-based design approach has led to significant gains in motor power density and efficiency [3]. However, a truly optimized design for a particular application cannot be obtained without taking into account nearly every single aspect of the application and its constraints. For example, in an aircraft application, it is crucial that the motor should fit inside the

available space (and the space taken up should be properly utilized), spin in an RPM range dictated by the propellers, operate at a voltage level dictated by the rest of the power system, and so on. A system-level optimization approach implies incorporating these considerations into the multiphysics motor design process. The addition of these considerations to the multi-physics optimization approach enables new avenues for increasing power density and efficiency of electric machines.

1.2 Motivation

The research work for this thesis was motivated by a large-scale design study on regional hybrid-electric aircraft for the FUTPRINT50 Project [10]. The large scale design study involved analyzing electric motor capabilities for a wide range of power, voltage, and RPM cases. Early on in the project, it was decided to use the slotless, outer rotor, permanent magnet synchronous motor topology as a basis for this design study, since prior research efforts [6] have shown that this motor has best-in-class power density and efficiency and is particularly suited to the needs of electrified aircraft propulsion. However, existing analytical models available at the time were incapable of predicting motor capabilities across the wide design space desired, and an improved analytical model was needed.

In this thesis, we present this improved analytical model of a slotless high-frequency permanent magnet synchronous motor that includes the aircraft system level considerations. As such, particular focus is provided to the elements that are most affected by these considerations, such as the insulation design, thermal management and heatsink design, structural components etc. The key research questions that this thesis sets out to answer is:

- How does the addition of these considerations impact the maximum obtainable power density and efficiency of the electric machines?
- What are the new tradeoffs that occur in the new sizing models?

1.3 Organization of this Thesis

This thesis is broken up into 5 chapters. Chapter 1 introduced the background, motivation and research questions that are being addressed in this thesis. Chapter 2 discusses the modelling, considerations, and the optimization process. A broad design exploration was conducted as part of the research for this thesis, and some results are provided in Chapter 3. Chapter 4 breaks down the key insights obtained from this design exploration, and discusses the key trends in motor Key Performance Indices (KPI's), along with some comparisons to prior optimization efforts. Chapter 5 concludes with some remarks on the shortcomings and the future work needed to address them.

CHAPTER 2

MODELLING AND OPTIMIZATION

This chapter describes the structure of the motor and the developed models. The motor under analysis here is a Outer Rotor, High Frequency, Low Inductance Surface Permanent Magnet Synchronous Motor developed by researchers at the University of Illinois at Urbana-Champaign. The motor is designed for aerospace propulsion applications and boasts of best-in-class power density, efficiency, and many other KPI's[11].

Section 2.1 describes the structure and geometry of the motor, and gives a brief overview of the mechanical aspects of the motor. Section 2.2 discusses the electromagnetic operation and loss mechanisms in the motor, and their computation. Section 2.3 describes the insulation design and winding design strategies employed for enabling high-voltage operation. Section 2.4 discusses the design of the heatsink with the approach used for its scaling. Section 2.5 describes the sizing of the gearbox and other structural elements. Section 2.6 shares details on the process of integrating the mission profile of an aircraft into the optimization process, and Section 2.7 describes the optimization process used.

2.1 Machine Structure

The basic machine structure is described in [6]. Figure 2.1 shows the structure of the outer-rotor surface permanent magnet (PM) motor design. The dimensions of all the elements are optimized (using the process described in Chapter 2.7) to provide a specified output power at the motor shaft. The multi-objective optimization process outputs a Pareto Front of designs that maximize specific power and efficiency. The pareto front plots shown across this thesis are scatter plots, where each point represents one machine design. The following subsections give a high-level overview of the machine sizing

model.

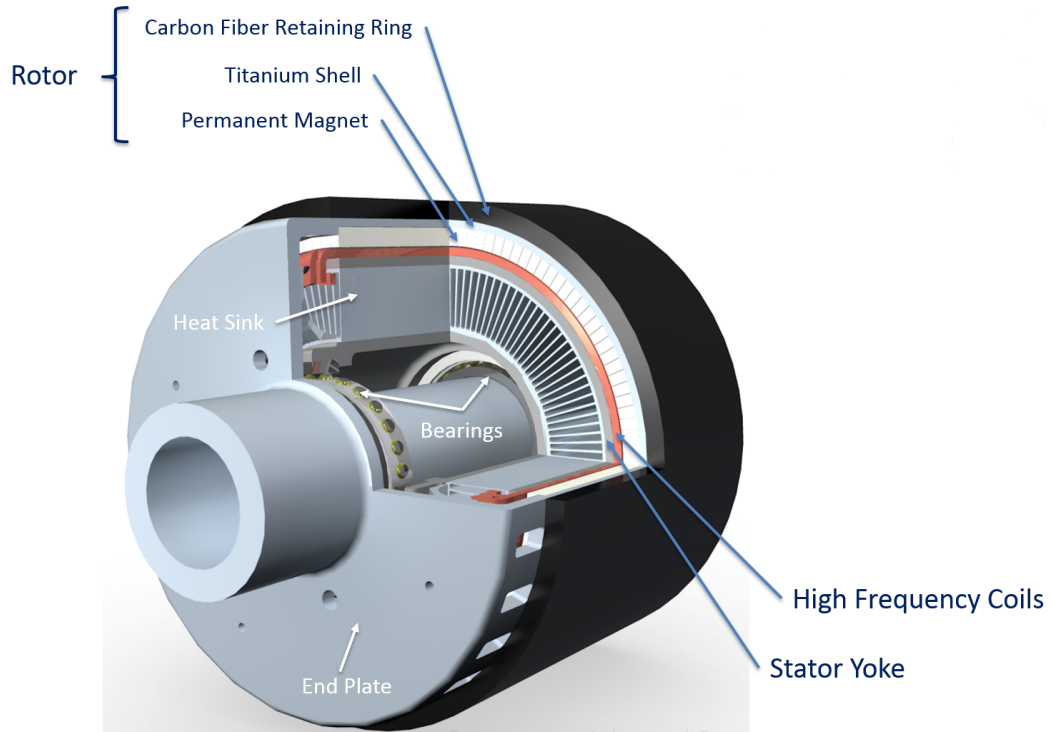


Figure 2.1: Structure of the High-Specific Power Slotless Motor

2.2 Electromagnetics & Loss Mechanisms

The machine magnetic field is created by the Halbach array of permanent magnets on the rotor, which form a near-perfect sinusoidal magnetic field waveform in the airgap. The expressions for the radial and tangential magnetic flux density in the airgap and winding region is given in [12], and the radial magnetic flux density expression is reproduced below in equation 2.1. For purposes of the optimization model, only the peak value of the radial component is essential, since the tangential component varies with time as the motor rotates.

$$B_{radial} = \frac{4B_r}{D_0} \frac{p}{1-p} (1 + u_r) \left[1 - \left(\frac{R_r}{R_m} \right)^{p-1} \right] \left[1 + \left(\frac{R_i}{r} \right)^{2p} \right] \left(\frac{r}{R_r} \right)^{p-1} \quad (2.1)$$

Using the Lorentz Force Law, the average torque is obtained as shown in equation 2.2:

$$T_e = \frac{4\pi B_{rem} J_{s.pk} L}{D_0} \frac{p}{1-p} (1 + u_r) \left[1 - \left(\frac{R_r}{R_m} \right)^{p-1} \right] \left[\frac{1}{p+2} \frac{R_w^{p+2} - R_{sy}^{p+2}}{R_r^{p-1}} + \frac{1}{2-p} \frac{R_{sy}^{2p}}{R_r^{p-1}} (R_w^{2-p} - R_{sy}^{2-p}) \right] \quad (2.2)$$

The losses in the motor are primarily from the DC and AC losses in the windings, the loss in the stator iron and the windage losses on the airgap and outer rotating surfaces, and the power consumed by the fan to drive the cooling air through the heatsink.

DC Loss is the ohmic loss in the winding conductors, and is proportional to the square of the current density and the volume of the conductor. AC Loss occurs due to the strand eddy current losses due to the changing magnetic flux density across the winding conductors, and the methods from [13] are used for computing it.

Iron losses in the stator yoke are computed using modified Steinmetz equations for the iron losses as given in [14] [15], and the loss coefficient data for the different possible materials is specified in [16]. Friction losses at the outer and airgap surfaces occur due to the turbulent flow of air from the high-speed rotation of the machine. Friction losses at both rotating surfaces are computed using methods defined in [17].

The cooling fan also consumes power in blowing air through the heatsink. The fan for the motor is assumed to be designed as per the methods specified in [18]. The power consumption of the fan is proportional to the mass flow rate, the pressure drop, and the velocity of air as it travels through the heatsink. It is assumed that for the various different motor designs, the fan design can be tweaked to provide the desired air velocity, which is 20m/s.

For the 1MW size designs considered in this thesis, results for fan power consumption from [19] are used as a reference.

2.3 Winding & Insulation Design

The design of the insulation system is critical in determining both the performance and reliability of the motor. The insulation around the motor high-voltage windings must be thick enough to prevent fatal partial discharge from occurring across the phase windings or to ground, especially in an aerospace environment, and yet must be thin enough to avoid impeding the heat transfer from the conductors to the heatsink. As will be seen later, the power density of slotless electric machines is particularly sensitive to insulation thickness, as the insulation has a much larger impact on thermal conductivity from the windings to the heatsink.

For aircraft propulsion applications, prior research [20] has shown that the use of voltages above the current $\pm 270\text{V}$ DC can be beneficial in improving the power density of the aircraft power transmission system. At megawatt ranges of power, using lower voltages can lead to impractically large and heavy power cables. Thus, to cover a wide range of possible operating voltages, the insulation system design in this thesis considers voltages from 700V DC to 5000V DC. The assumption here is that the motor phase voltages are obtained by a power-electronic inverter operating using Space Vector Modulation (SVM), at a modulation depth of 1. The motor stator coil back EMF is computed using the methods described in [21], and the coils are arranged in series and parallel combinations to yield the motor phase voltage corresponding to DC operating voltage.

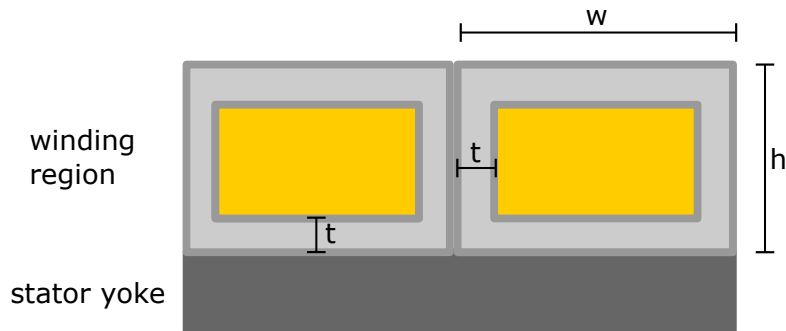


Figure 2.2: Winding Insulation Model Diagram

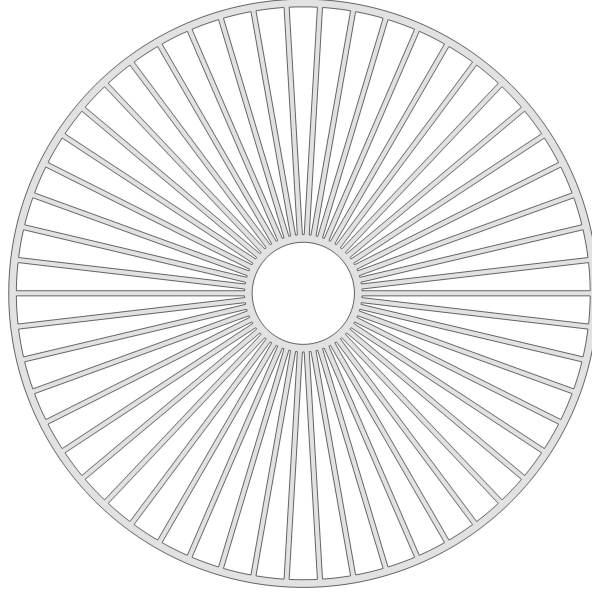


Figure 2.3: Heatsink Cross Section

Figure 2.2 shows the homogenized winding region cross section model used by the tool to size the thickness of the insulating resin. The width and height of each winding (denoted by w and h respectively in the figure) is determined by the sizing of each motor. The slot width w is determined by dividing the outer circumference of the stator with the number of slots (which is 6 times the number of motor poles). The height h of the winding region is a free variable in the motor sizing model, and thus is selected by the optimization algorithm in each run. The thickness t of the insulation is determined by the voltage that the motor needs to operate at. The desired rated operating voltage is taken as an input by the optimization algorithm. The insulation is sized according to the methods presented in [22]. The insulation is sized to operate at pressures of 0.2 atm and temperatures of 180°C. At these conditions, the breakdown electric field of air is approximately 1.6KV/mm. After a safety margin of 40%, the maximum permissible field across the insulation is 1 KV/mm. The insulation thickness is scaled to maintain electric field under 1 KV/mm for all cases of operating voltage, so that any air inside the insulation due to imperfect impregnation does not break down.

Using this process, the fill factor of the winding is computed. The fill factor is the area of the conductor (shown in yellow in the figure) divided by the total area of the slot ($w \times h$). For manufacturing as well as thermal related

reasons, a minimum constraint on the fill factor is applied. The constraint is selected such that the optimization process can find viable candidate designs at very high voltages while remaining within manufacturable limits.

With regards to the thermal conductivity of the winding structure, it is suggested in [23] that a single turn winding has better thermal conductivity as compared to a multiple turn winding, as the turn-to-turn insulation leads to significant degradation in the overall thermal conductivity of the winding structure. The conductor region (shown in yellow in Figure 2.2) is a composition of litz conductors, the conductor polyimide insulation and the impregnated resin. The bundle is assumed to be homogenous for the purposes of computing equivalent thermal conductivity, and the process to find the bundle thermal conductivity for impregnated litz wire windings is present in [24]. Since thermal conductivity of the windings is a key factor in achieving high power density, a single turn winding structure is adopted for all designs, which is same as the structure shown in Figure 2.2. The reduction in insulation material required by the single turn winding design greatly improves the thermal conductivity and heat transfer capabilities of the windings, permitting higher current densities to be achieved.

2.4 Heatsink Design

Accurate and reliable thermal management of the motor is key to achieving high power density. Due to the requirement of low computational complexity needed for a large-scale optimization, a 1D thermal circuit at steady state is used to determine the temperatures at various points in the stator[25]. The class H insulation rating puts a maximum cap of 165C on the winding temperature after considering the safety buffer, so as to not degrade the insulation prematurely. Since the heatsink transfers heat to the forced airflow via convection, standard heat transfer coefficients from literature were used for forced airflow at a moderate velocity [26][27], which is held constant throughout all studies in this thesis.

To appropriately scale the thermal capabilities of different designs and to utilize the stator volume effectively, the heatsink design is varied during the optimization. Figure 2.3 shows the cross section of the heatsink. The inner diameter of the heatsink cylinder is fixed to the shaft and bearings, and

the outer diameter can vary freely with the stator yoke dimensions. Hence, the radial length of the heatsink fins varies for different motor designs. The number of heatsink fins control the heatsink weight and surface area. A larger number of fins ensures more area for heat transfer at the cost of a heavier heatsink. Thus, the optimization arrives at a heatsink design that balances thermal requirements with minimum mass.

2.5 Structural Components & Gearbox Considerations

Since mechanical design considerations & requirements can vary significantly depending on the size, speed and power rating of the machine, the optimization fitness function attempts to estimate the weight of the structural components such as the shaft, endplate, bearings etc using scaling from previously manufactured designs [28][29]. To estimate the weight of aerospace applicable gearboxes across a range of different power ratings and reduction ratios, an algorithm developed by the NASA Glenn Research Center based on the survey of many existing aircraft application gearboxes, was used [30]. The relations are:

$$Index = \frac{HP^{0.76} \cdot RPM_{in}^{0.13}}{RPM_{out}^{0.89}} \quad (2.3)$$

$$W_{gb} = Index \cdot K_{gb} \cdot (0.454Kg/lb) \quad (2.4)$$

The technology scaling factor K_{gb} was determined for advanced future gearboxes based on projections from the survey. Other methods for finding the weight of reduction gearboxes can be found in [31].

2.6 Mission Profile

During a typical aircraft flight mission, the electric machine will operate at various RPM and torque levels. For accurate prediction of the machine suitability for the particular mission, the efficiency of the electric machine must be evaluated throughout the entire operating range. The efficiency map of the machine determines the machine losses for each RPM/torque combination, and this is used in conjunction with the mission profile to determine

total machine energy loss in the mission. The mission profile used as an example here is described in [32], and is specified as a table of RPM and torque values in PU for different stages of the mission, along with the time spent in each stage. Each RPM / torque operating point has an efficiency associated with it, and the time spent at that operating point can be used to compute the machine losses and the total energy loss across the entire mission. If desired, the total energy loss can be used as an objective in the optimization process instead of the efficiency at rated conditions. An example of this is provided in the discussions in Chapter 4.

2.7 Optimization Process

An evolutionary genetic algorithm was used to optimize the motor model, and a MATLAB toolbox GOSET [33] was employed for this purpose. The optimization has two objectives - to maximize specific power and to maximize efficiency. All the results shown in this thesis were generated with 10000 individual, 15000 generation optimization runs. In the cases where the motor is being optimized over a specified mission profile, the efficiency objective is replaced by the total loss across the mission, which is minimized. The design objective functions are:

$$\begin{aligned} \max_x \quad s.p.(x) &= \frac{P_{out}}{Mass(x)} \\ \eta(x) &= \frac{P_{out}}{P_{in}(x)} \end{aligned} \quad (2.5)$$

Where $s.p.$ represents the specific power of a design x , P_{out} is the output power and $P_{in}(x)$ is the input power after accounting for all losses.

Nine design variables are selected: the outer radius (R_o), magnet thickness (D_m), winding region thickness (D_w), RPM, current density (J_s), stator yoke thickness (D_{sy}), pole pairs (PP), heatsink fin count (N_{fins}), and stator yoke material (M_{SY}). Hence, the design variable vector can be specified as:

$$x = \{R_o, D_m, D_w, RPM, J_s, D_{sy}, N_{fins}, PP, M_{SY}\} \quad (2.6)$$

The DC network voltage can be specified as a design variable in the above vector as well. However, in many applications, the network voltage is usually

not a variable that the motor designer can freely select. The network voltage selection is based on a large set of requirements that do not solely depend on the motor. Hence, the DC voltage is taken as a fixed (but user specified) parameter in the optimization process.

If desired, additional free variables can be added to extend the design space. For example, if the application at hand necessitates the use of a fixed shaft rotational speed, a design variable can be added to the vector x that specifies if a gearbox is used or not. The weight of the gearbox can be computed from the methods described earlier and added to the total motor weight, to compute the motor + gearbox subsystem power density. This can be compared with a direct drive motor which does not need a gearbox to determine the better solution for the specific application. Comparison results are shown in the following chapters. Similarly, other design variables can be added to extend the capabilities of the optimization tool.

The upper and lower bounds on the selected design variables are adjusted according to the design requirements. Constraints on the retaining ring thickness, tip speed, saturation flux density of the yoke (dependent on selected material), winding fill factor and maximum winding temperature are placed in accordance with physical and manufacturing limits, and are specified below:

- Rotating Tip Speed

$$\omega_m \cdot R_o \leq 343m/s \quad (2.7)$$

- Stator Yoke Saturation Flux Density

$$B_{stator_yoke} < B_{sat} \quad (2.8)$$

- Hotspot Temperature

$$T_{max} \leq 165C \quad (2.9)$$

- Retaining Ring Thickness

$$D_{rr} \leq 25mm \quad (2.10)$$

- Winding Fill Factor

$$FillFactor \geq 0.1 \quad (2.11)$$

CHAPTER 3

DESIGN SPACE EXPLORATION STUDY

For the purpose of testing the applicability of this optimization model, a large scale design exploration was conducted for a 50-passenger hybrid-electric aircraft from the FUTPRINT50 project.

To ensure that all important design cases were covered, the range of the exploration was set as follows. A set of cases of motor power, RPM and voltage were defined, and the optimization run for each of them to obtain a pareto front of candidate designs and to evaluate electric motor capabilities. The design sets were:

$$Power = \{50, 100, 150, 200, 300, 400, 500, 600, 800, 1000\} KW$$

$$Voltage = \{700, 100, 1300, 1600, 1900, 2200\} V_{DC}$$

$$RPM = \{1000 - 1200, 5000 - 30000\} RPM$$

Each point from these vectors was selected to create one design case, for a total of 120 design cases. For each design case, an optimization run was executed to obtain the specific power and efficiency tradeoff curves, for different parameters. Some of these plots are presented here, which enables us to identify and analyse the trends in motor capabilities across a wide range of power, voltage and RPM cases.

3.1 Trend Analysis & Pareto Fronts

3.1.1 Power

For comparing how motor performance scales with changes in the output power rating, we consider 3 cases in particular: 50KW, 500KW and 1MW, such that we have an even spread across the whole power spectrum. For these 3 cases, the RPM was fixed to the high speed case, i.e 5000 - 30000 RPM, and the voltage was fixed to 700V DC. The results are shown in figure 3.1

Surprisingly, the peak power density capabilities do not change significantly as the motor rated power is dropped from 1MW to 500KW, and only drops significantly below that. This means that for large motors with ratings in the multiple hundreds of kilowatts, the optimization algorithm is able to find avenues to maintain power density. From these pareto fronts, one such avenue is obvious; the peak motor RPM rises inversely with the power rating. For the 1MW case, the peak RPM is around 21,000, by 500KW, it rises to around 24,000, and by 50KW, the RPM pushes against the 30,000 RPM limit, indicating that it would need even higher speeds to maintain power density. The rotor shear stress is also an indicator of this phenomenon. At low power levels, the motors are small, indicating that insufficient current density, magnetic loading, and thermal management is available for developing high rotor shear stresses. Thus, the torque per rotor volume (TRV) is low, indicating that the motor must spin at very high speeds to develop the needed power. As the motors power ratings and size grows, there is sufficient volume for maintaining magnetic loading and current density, thus the rotor shear stress and power density cap out at a certain limit.

An additional insight that can be noted is that this peak power density appears at a severe cost to efficiency. The maximum power density designs of the 50KW rating have efficiencies as low as 94.2%, and this efficiency rapidly increases at higher power levels.

3.1.2 Voltage

A similar exercise was performed for voltage analysis. We consider 3 cases in particular: 700V, 1600V and 1900V. All these 3 cases are for the 1MW power

level at high speed (5,000 to 30,000 RPM). All other design parameters were kept as identical for an even comparison. The results are shown in figure 3.2

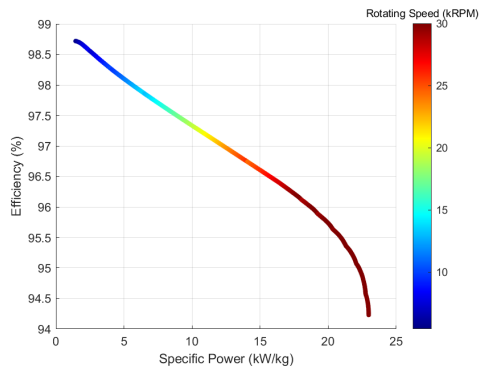
For this comparison, the slot current density is used on the color axis, to highlight the main impact of the increasing voltage. After a base point of minimum manufacturable thickness, increasing the voltage will lead to use of additional encapsulating resin (which is the main winding insulator), thus reducing the overall winding fill factor and overall winding bundle thermal conductivity. This is clearly reflected in the the pareto fronts shown here; as the voltage is increased, the total slot current density reduces proportionally. Also clearly visible is the impact on the electric loading of the motor, which too drops significantly as the voltage is increased. It is interesting to note that the maximum electric loading and the maximum current density do not occur at the same points on the pareto front, i.e. the design with the highest current density does not have the highest electric loading, and vice versa.

3.1.3 RPM

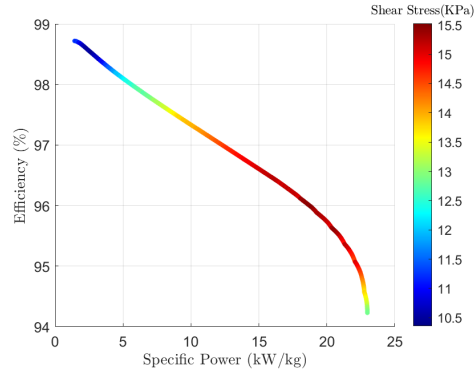
Here, the low-speed and high speed designs are compared, when the motor power ratings and voltage ratings are fixed. We consider here the case where the motor power is fixed to 1MW, and the voltage is fixed to 700V. The RPM constraints are locked to the 2 cases, and the resulting pareto fronts are shown in figure 3.3.

It is clear from these pareto fronts that the low RPM limits of 1,000 to 1,200 RPM severely limit maximum motor capabilities. The maximum achievable power density gets dropped from over 30 KW/Kg down to merely 11KW/Kg, which is a reduction of nearly 3x. This can be explained using the maximum achievable tip speed, and the tradeoffs needed to achieve that. Tip speed is essentially the maximum linear velocity of the outermost rotating part of the motor and is a product of the motor radius and its angular velocity. For the low speed case, the angular velocity of the motor is constrained to be only around 1200 RPM, which is extremely low. It can be clearly seen that in the low speed case, nearly all designs are at the upper bound of 1200 RPM, whereas in the high-speed case, no design even comes close to the upper bound of 30,000 RPM. This means that the low speed motors need to have an extremely large outer radius, which means all the structural parts

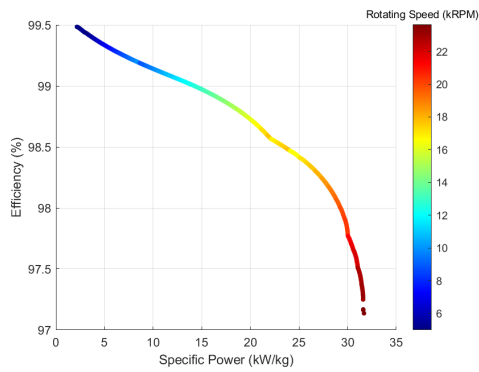
get larger and heavier, which in turn reduces power density. This is also a particularly a concern in outer-rotor machines utilizing a cantilevered rotor architecture, which needs to have a mechanism for torque transfer to the inner shaft from the outer rotor, which is usually achieved by the means of a plate connected to both parts on one axial end of the motor. This tradeoff is clearly reflected in the tip speed that is plotted in the color axis of the pareto fronts. The high-speed motor achieves a tip speed over 2.7 times that of the low speed motor, which also tracks well with the increase in power density achieved. However, the low speed has benefits in lower aerodynamic losses at the rotating surface, thus achieving better efficiency.



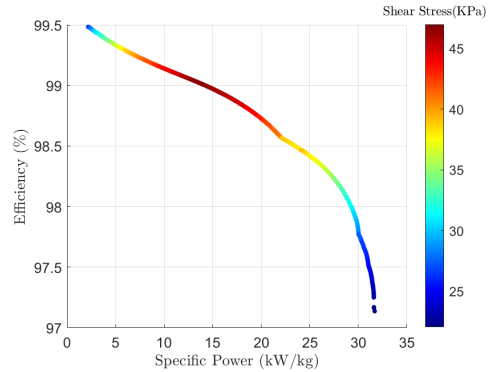
(a) 50KW RPM



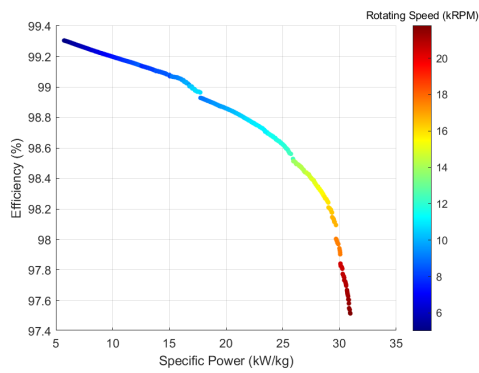
(b) 50KW Shear Stress



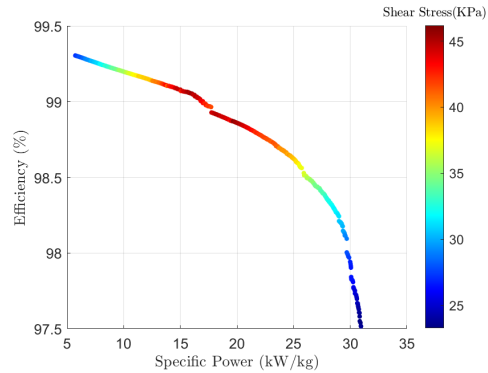
(c) 500KW RPM



(d) 500KW Shear Stress



(e) 1MW RPM



(f) 1MW Shear Stress

Figure 3.1: Comparison of Motor Pareto Fronts at different power levels

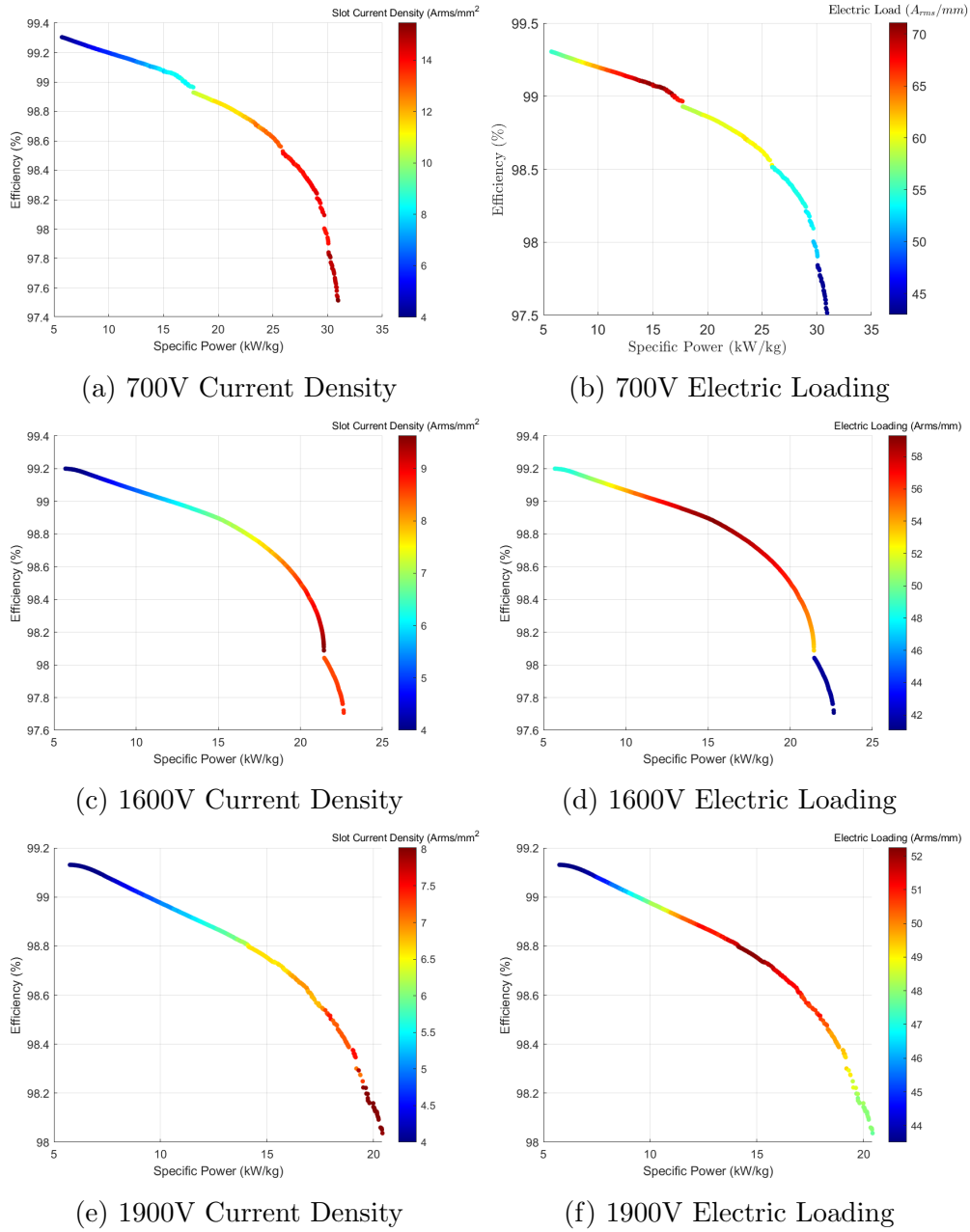
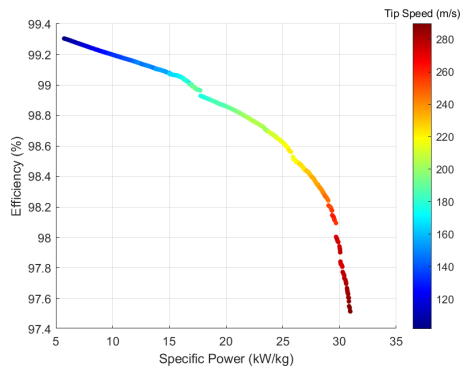
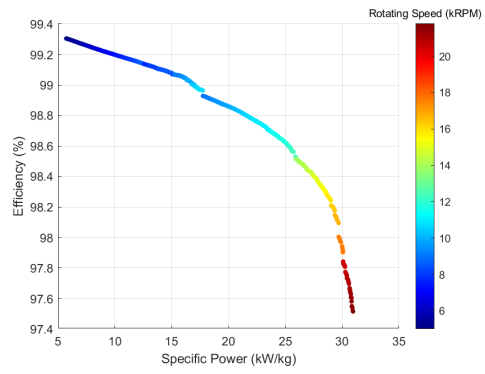


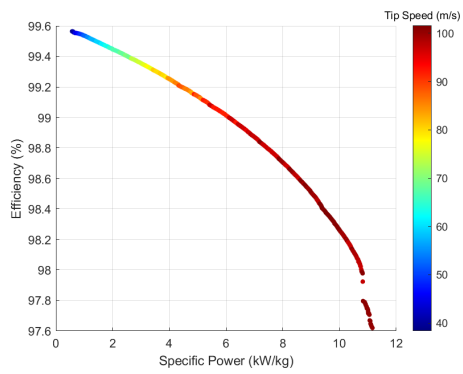
Figure 3.2: Comparison of Motor Pareto Fronts at different voltage levels



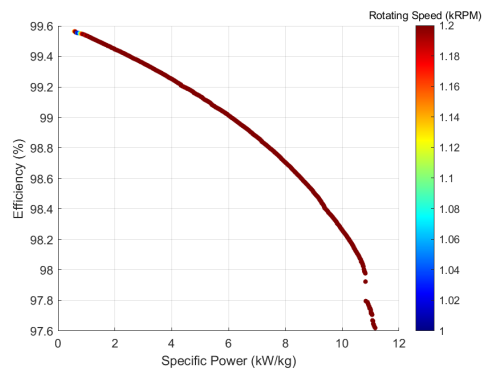
(a) High Speed - Tip Speed



(b) High Speed RPM



(c) Low Speed - Tip Speed



(d) Low Speed RPM

Figure 3.3: Comparison of Motor Pareto Fronts at different RPM cases

CHAPTER 4

KEY INSIGHTS & DISCUSSION

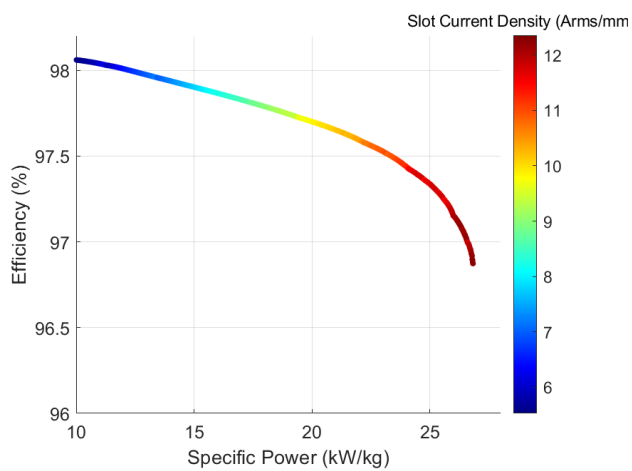
Through the use of the machine optimization tool described in this thesis, a few key findings are presented. One, the impact of increasing the machine rated voltage on the power density, efficiency and other key parameters are discussed. Out of all the parameters, the most important one to analyze is the permissible current density in the winding slot, as that is determined by the heat transfer capabilities out of the windings, which the insulation and voltage rating directly impacts.

The second is the comparison of motor capabilities at different RPM ranges. This is crucial for assessing direct-drive motors versus high-speed motors coupled to a reduction gearbox. While motor power density can be increased by increasing rotation speed, the corresponding increase in reduction gearbox weight may offset this, and thus the high-speed motor may not have the best system-level power density in all cases.

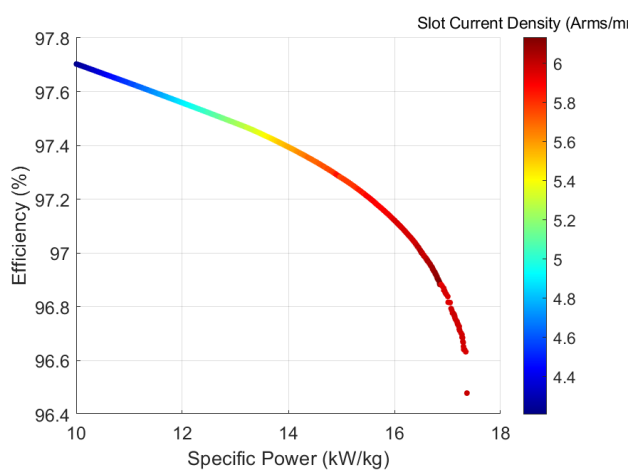
Third is to evaluate the impact of mission profile considerations. Since the electric machine will not have the same efficiency throughout its operating range, total loss across the mission is key for assessing electric motor suitability. And fourth is to assess the improvements from prior optimization efforts, and understand where the improvements are coming from. Lastly, based on this understanding, some general remarks on increasing power density and efficiency are provided, along with high-level approaches to making that happen.

4.1 Comparison Pareto Fronts

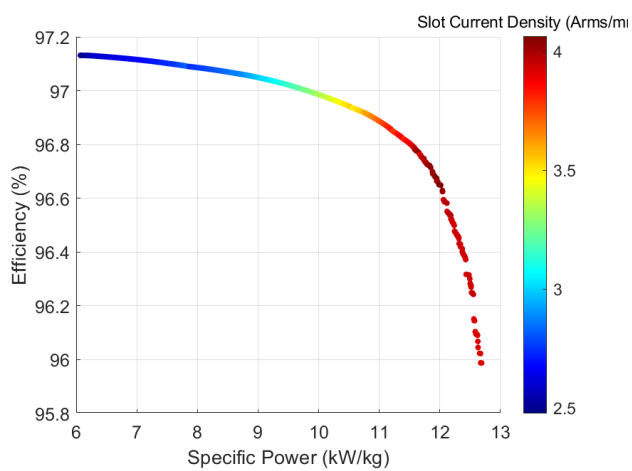
While the previous chapter showed the broad trends from the design space exploration, many of the trends observed require a deeper, dedicated analysis to thoroughly understand. For this, another set of design optimizations was



(a) 700V

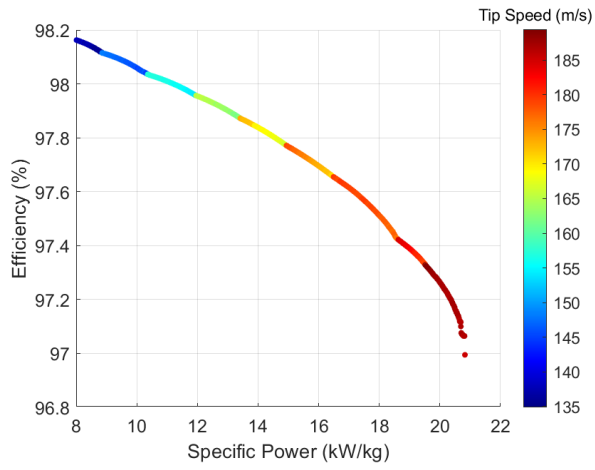


(b) 3000V

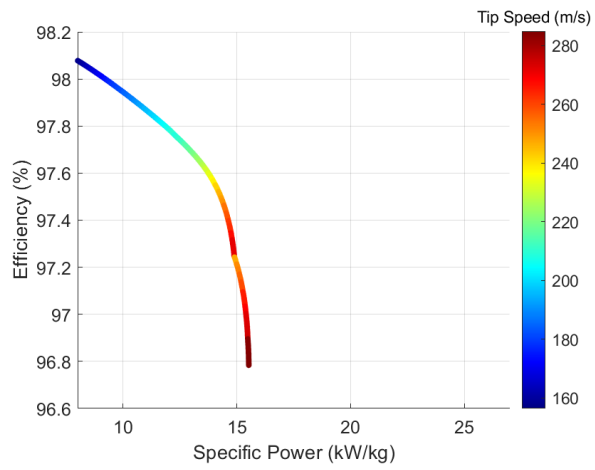


(c) 5000V

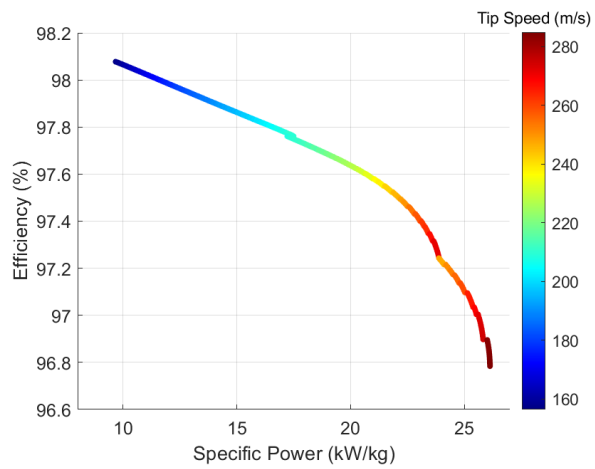
Figure 4.1: Voltage Comparison



(a) Low Speed Direct Drive



(b) High Speed with Gearbox



(c) High Speed without Gearbox

Figure 4.2: Direct Drive vs High Speed Reduction Drive

run, broadening the voltage range from 700V-2200V to 700V-5000V. The higher voltage range shows the impact on the motor parameters and power density much more clearly.

The Pareto fronts of figures 4.1 and 4.2 show the tradeoffs in specific power and efficiency for different target cases of Voltage & RPM respectively. All plots are for designs with rated power of 1MW.

In Figure 4.1, a low voltage (700V) design is compared with a medium voltage design (3000V) and a high voltage design (5000V). It can be seen that the lower voltage designs are able to achieve much higher current densities than the high voltage ones. This effect is particularly pronounced for 5000V designs. This is due to the insulation being much thicker for preventing partial discharge, thus severely impeding heat transfer to the heatsink. Due to the placement of the windings in the airgap, radial depth is limited and insufficient cross section area is available for thicker windings and larger conductors. The reason behind this is that radially thicker windings increase the effective airgap depth in the magnetic equivalent circuit of the motor pole, thus severely reducing the amount of flux that links to the windings from the permanent magnets. While this is beneficial from one aspect, that a lower stator yoke depth would be required to carry that flux, the reduced flux density *and* the reduced current density means that it is incredibly difficult for the motors to generate any torque. This is a trait that especially affects slotless machines, and the placement of the windings in the airgap instead of slots is the prime culprit. In slotted machines, the stator teeth link the flux from the rotor, thus the flux density in the center of the winding loop is almost always equal to the saturation flux density of the stator iron (around 1.8 to 2 T). In case of slotless machines, the flux density around the winding loop is much lower (1T at best, usually around 0.7T to 0.8T). This implies that slotless machines inherently start with a disadvantage; they must find ways to increase current density to make up for the shortfall. High voltage windings with thicker insulation directly affects that; thus the power density drops much faster with voltage as compared to slotted machines. The only remaining way to increase the torque rating is to use a larger diameter and axial length, which reduces specific power.

Figure 4.2 compares a low speed direct drive (500-3000 RPM) case with a high speed (10000 - 25000 RPM) case, both with and without a gearbox. It can be observed that the low-speed case yields designs with better efficiency,

but the high-speed case yields higher power density. This is explained by the low-speed cases requiring higher rated torque, and thus have electromagnetic interactions occurring at larger radii. This increases the weight of inactive structural components. The lower speed reduces the frictional losses at the rotating surfaces and helps increase efficiency. The addition of a gearbox adds significant weight, particularly when the reduction ratio is so large. This implies that when the application demands a low speed drive at very high power levels, there may be significant advantages in going with a direct drive solution, as the reduction gears will add significant weight.

The additional degrees of freedom enables the algorithm to maintain much of the power density under challenging design requirements, such as low RPM and high voltage. In figure 4.1, a 7x increase in voltage (and thus insulation thickness), going from 700V to 5000V only leads to an approximately 3x reduction in current density & approximately 2x reduction in maximum specific power, implying that the optimization process finds other avenues for weight reduction. Similarly in figure 4.2, reducing the upper bound on RPM by 8x only reduces the tip speed by approximately 35% and maximum specific power by 20%.

4.2 Mission Profile Analysis

Figure 4.3 shows the efficiency map of one design obtained from the optimization. It can be seen that the machine is most efficient at medium to high power output levels, and that efficiency reduces significantly as either the RPM and Torque are reduced further. Similar maps are generated for every design on the optimal Pareto Front, and the total energy loss for each is computed and shown in Figure 4.4.

It can be seen that the total loss in the overall aircraft mission increases along with the specific power of the motor and correspondingly reduces as the machine efficiency increases. This indicates that the machine efficiency at peak rated conditions is a strong indicator of the total energy loss across the mission. This can also be inferred from the efficiency map, as large regions of the machine's operating range has efficiency close to its maximum. While the results shown here have data for only one machine and optimization cycle, this can be applied to other cases to obtain application-specific results.

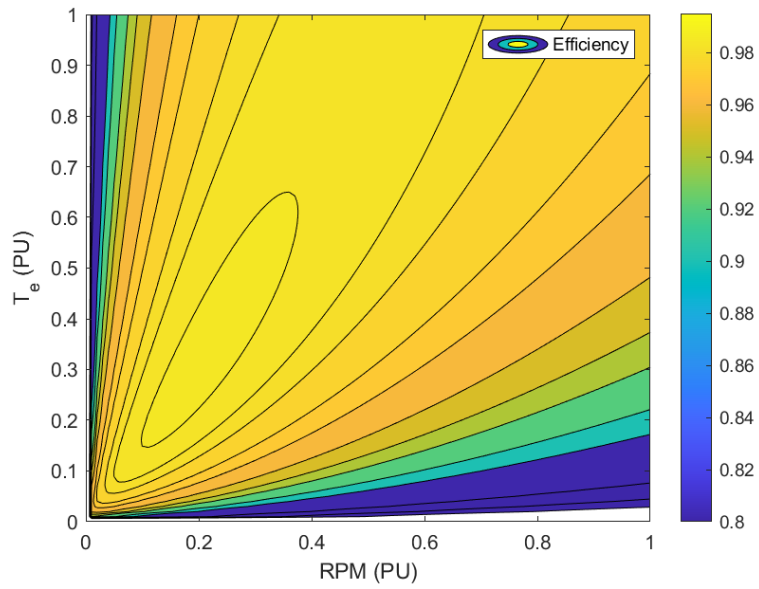


Figure 4.3: Efficiency Map for an example machine design

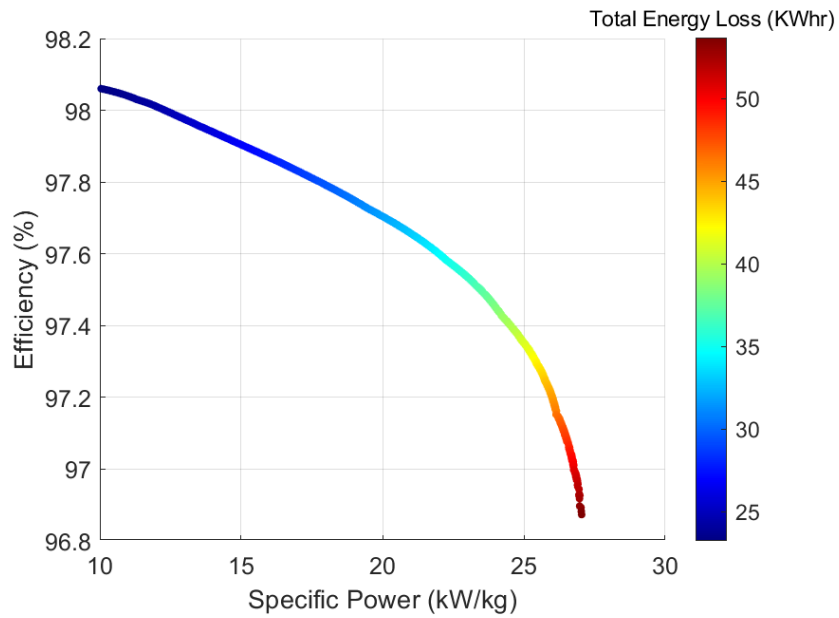


Figure 4.4: Pareto Front of Total Energy Loss in the Mission

4.3 Improvements from Prior Efforts

Here, the results obtained from the improved algorithm is compared to prior approaches demonstrated in [2]. Figure 4.5 shows the two pareto fronts of power density vs efficiency. For a proper comparison, the upper and lower bounds of design variables common to both approaches are fixed to the same values, which are presented in equation (16) in [2].

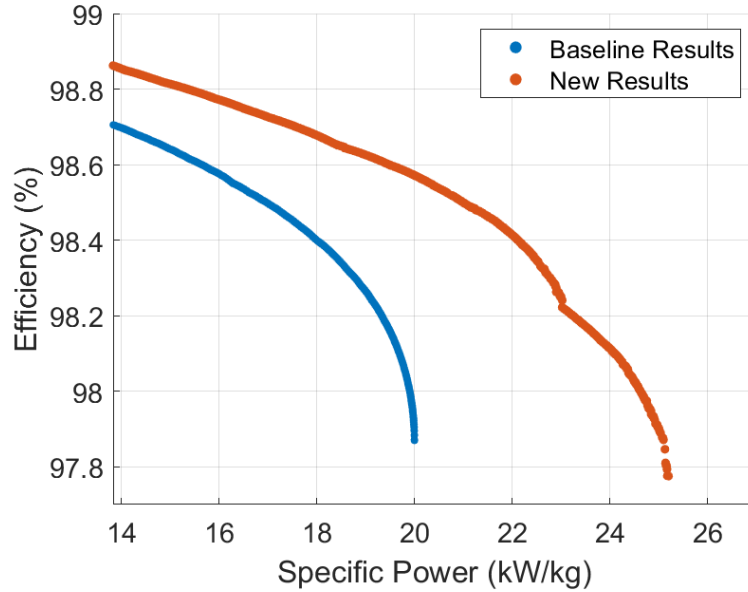


Figure 4.5: Comparison between results of [2] and this thesis

It can be seen that the new approach leads to a power density improvement of approximately 26% when considering designs prioritizing power density. On the other end, maximum efficiency increases from 98.7% to 98.85% for designs that prioritize efficiency. For the comparison data in tables 4.1 and 4.2, the most power-dense designs are selected. The weight breakdown of the individual components is given in Table 4.1, and a comparison of key motor parameters is provided in Table 4.2. The key weight differences are in the permanent magnets, windings and the heatsink. It should be noted that the designs in this thesis account for structural components such as the shaft, endplate, bearings etc. that were not accounted for previously.

The reasons for improvement are apparent from the performance parameters in Table 4.2. The new motor develops a higher shear stress on the rotor surface and has much higher electric loading than the one from [2]. That

combined with the higher rotating speed, develops much higher power per unit length, leading to a reduced stack length and thus higher power density.

Table 4.1: Weight Breakdown Comparison

Component	From [2]	This Thesis
Retaining Ring	1.54 kg	3.62 kg
Titanium Shell	3.02 kg	2.99 kg
Permanent Magnets	16.36 kg	10.98 kg
Windings	7.02 kg	4.08 kg
Stator Yoke	9.24 kg	4.45 kg
Heatsink	11.67 kg	6.3 kg
Ground Cylinder	1.14 kg	1.14 kg
Other Structural Components	-	6 kg
Total	50.01 kg	39.67 kg

Table 4.2: Comparison of Key Motor Performance Parameters

Key Parameters	From [2]	This Thesis
Specific Power (KW/Kg)	20	25.2
Slot Current Density (A_{rms}/mm^2)	12.03	10.5
Airgap Flux Density (T)	0.97	0.69
Rotor Shear Stress (KPa)	23.66	30
Electric Loading (A_{rms}/mm)	36	65
RPM	15970	19176
Tip Speed (m/s)	247	308
Pole Pairs	10	10
Axial Stack Length (mm)	233.7	174.4
Electrical Frequency (Hz)	2662	3196
Stator Yoke Material	HiperCo 50	Vacoflux 48
Lamination Thickness (mm)	0.15	0.05

This is somewhat surprising, considering the fact that this is achieved by the means of a slightly lower current density and much lower airgap flux density. This can be understood by analysing the tradeoffs that occur when trying to increase both these quantities. To obtain a larger airgap flux density, a thicker ring of magnets is required, which adds increased stresses to the retaining ring and increases weight, thereby reducing the maximum achievable tip speed. It can be understood that to achieve this level of power

density, inclusion of additional permanent magnet material to the rotor is counterproductive.

However, increased current density does not come with a direct increase in weight, which was the case with flux density. But, increased current density does come with additional thermal management challenges, which requires a larger and heavier heatsink with additional surface area. It should be noted at this point that all designs on the pareto front have hotspot temperatures that converge to the specified limit of 165C, and thus attempting to increase current density will require a larger heatsink. After a certain point, any additional current density does not provide sufficient additional torque to counteract the corresponding increase in weight, and the efficiency penalty of higher conductor losses means that any design with higher current density is non-dominant and does not show up on the Pareto front.

Thus, the only remaining way to increase power density is via increases in tip speed and electrical frequency. The tip speed of the new proposed design is nearly 25% higher and the electrical frequency is 20% higher, which tracks well with the 26% increase in power density. Reducing permanent magnet weight and increasing tip speed till the rotor material mechanical limits should provide commensurate gains in power density. Similarly, increasing electrical frequency and reducing yoke thickness till saturation and loss limits will also provide gains in power density. The tradeoffs here are purely dependent on the maximum limits of the materials used, and thus, power density can be pushed further via improvements in material properties in these areas.

4.4 On increasing Specific Power and Efficiency

It was also shown through results in this and prior chapters that using a better and more comprehensive model for motor optimization can result in better power density under a much broader set of constraints. Compared to some prior approaches in motor optimization, this tool can find feasible designs with much lower weight and better efficiency, indicating that the additional degrees of freedom gained by the better models are being utilized thoroughly. It also shows that conventional (i.e. non-superconducting) motors still have great potential for improvements over the current state of the art.

To put it simply, increasing the power density implies using lower quantities of relatively heavy materials such as iron, and substituting their use with lighter materials such as aluminium. In the context of the electric machines, this implies using high frequency and high pole count designs to reduce the quantity of steel used in the stator. [34] clearly notes this design strategy and shows its benefits to both induction and permanent magnet machines.

However, this concept can be extended to *any* heavy material used in the machine, albeit with different strategies. It should be noted that in terms of density, copper (at 8.2g/cc) and NdFeB permanent magnets (at 7.5g/cc) are very similar to the FeCo steel used in electric machines (at 7.85g/cc). Thus, material reductions in either the copper conductors or the rotor permanent magnets will bring similar benefits as reduction of steel, and minimizing all three is the key to achieving the best power density. This is enabled by the use of very high current densities, high electrical frequencies, and high tip speeds to minimize copper, steel and magnet weight respectively. Through this approach, the resulting thermal and mechanical stresses are transferred to the heatsink and retaining rings respectively, which are composed of lighter materials such as aluminium, titanium and carbon fiber.

Increasing efficiency, in a sense, is orthogonal to increasing power density. Increasing efficiency implies minimizing losses in the electrical machine, and the primary loss modes are losses in the conductors, iron and friction at the rotating surfaces. To reduce losses in the conductors, a lower current density must be used. Similarly, losses in the iron are greatly dependent on the electrical frequency of the motor, and lower frequency will yield lower iron losses. High tip speeds too imply high frictional heating and loss at the rotating surfaces. Thus, to maximize efficiency, current density, electrical frequency and tip speed will need to be minimized, which directly runs counter to increasing power density.

Thus, the aircraft designer must pick whether specific power or efficiency is of higher priority. This is determined by the size, payload, mission and other parameters of the aircraft. Particularly for hybrid electric aircraft applications, the trade-off between specific power and efficiency has implications on the total fuel burn of the aircraft. [35] performed a study for the conceptual design of NASA's high efficiency megawatt motor, and came to the conclusion that efficiency has a greater impact on fuel burn than specific power. Thus, their motor design focused on increasing efficiency as much as possible,

while maintaining weight at acceptable levels. While this conclusion may not remain the same for all aircraft, it at least provides a starting point to guide the design process for future aircraft and motor engineers.

CHAPTER 5

CONCLUSION

In conclusion, this thesis describes an improved electric motor sizing model for the design and optimization of aerospace-grade high specific power motors. By incorporating space, RPM, and voltage considerations into the sizing model, a larger, more comprehensive design space is explored for motor sizing. This is helpful for applications in distributed electric propulsion, where a large number of motors may be distributed along the aerodynamic control surfaces of the aircraft, necessitating that each motor be small, light and low-power. This tool can also help in executive decision-making at the beginning of the design cycle of new aircraft, by helping the decision makers to determine the best selections for their particular application.

5.1 Key Shortcomings & Challenges

While a great deal of progress has been made through this work on understanding the mechanisms by which the capabilities and limits of these motors are improved, the models developed are not perfect and there exist several avenues for improvement. Some of them are described here, in the hope that future researchers can develop improvements and increase the fidelity of the models presented in this thesis.

First of all, the outer rotor permanent magnet motor concept is particularly suited to high-speed applications. The cantilevered rotor style does not scale well to very large diameter designs, particularly because the endplate to transfer torque from the rotor to the inner shaft increases disproportionately in weight with the diameter of the motor. This is reflected in the results for the low RPM motors explored here; all designs struggle to achieve power density anywhere near to that of the high RPM designs. Thus, additional topologies for low RPM motors (such as Rim Drive designs) should be con-

sidered.

Secondly, the voltage & insulation scaling model adopted is based off a constant electric field assumption, which may not hold in practice due to manufacturing variances etc. For thicker insulation, there may be possibilities of imperfect manufacturing resulting in lower than expected voltage ratings of the windings. This is difficult to predict analytically; a large number of manufactured samples are required to develop a statistical model with any degree of accuracy. Thus, the results for the high voltage designs need to be validated much more thoroughly than the ones for the lower voltage designs. Lower voltage designs are much more common [36] and insulation manufacturing for low voltage motors is much more robust and reliable.

Next is the design of the cooling systems of the electric motors. It is assumed that the self pumped cooling method described in [19] is used for all designs, however, analytical relations for the scaling of the power consumption with varying heatsink geometry were not easily found. Thus, it was assumed that at the worst case, the power consumption would be similar to the 1MW motor described here, even for smaller motors. Thus, a uniform power loss penalty was applied to all the motors to account for the power consumption of the fan. This will not be accurate for smaller motors and disproportionately harms their efficiency. Analytical relations for the power consumption of the integrated centrifugal pump need to be developed for better accuracy. Similarly, the air velocity across the heatsink is considered constant regardless of the RPM range of the motor, assuming that the fan blade design could be changed to obtain this desired air velocity. This may or may not be possible in practice and practical upper and lower limits for this air velocity based on fan blade design and geometry need to be obtained.

An additional challenge that needs to be addressed at the detailed design stage is the rotordynamic behaviour of these motors. Currently, no rotordynamics analysis is performed in the analytical optimization models described here. Thus, it cannot be said for sure that these optimized machines will be stable and free from vibrations, particularly at high speeds.

Another aspect not considered in this work is the inclusion of a rotor thermal circuit. Performance of permanent magnet materials is highly dependent on their operating temperature, which can be quite high given the air friction losses of high speed machines. Thermal management of high-speed rotors is also extremely difficult. Thus, thorough understanding of the thermal be-

haviour and expected rotor temperatures is crucial. For this work, a magnet rated temperature of 180°C was assumed, and all magnet properties were set accordingly. However, the actual temperature of the magnets will deviate from this for many designs, and some mechanism must be included in future models to adjust the magnet properties based on some temperature estimates.

5.2 Future Work

This brings us to the future work for this project. While great improvements have been made to understanding and improving the design tool, it is by no means complete. Other than fixing the shortcomings described previously, there are several other avenues for improvements that are possible. For example, the cooling options so far are restricted to air cooled motors only. Adding the option of liquid cooled heatsinks to the toolbox is an important step to increase its flexibility. The toolbox also designs the motors purely in a mechanical sense, i.e. it does not generate an equivalent circuit or inductance values, which would be useful information for anyone attempting to design a drive inverter for such a motor. Drive inverters at high power levels, high voltage, and high fundamental frequency outputs are an active area of research, and electrical parameters of this motor would be a great asset to the power electronics and integration researchers. Particularly, due to the high fundamental frequencies of these designed motors and the limitations of high-power inverters, specialized control techniques such as complex controllers may be required. [37] has a thorough review and explanation of implementing these controllers on interior permanent magnet machines, and this technique can be implemented to drive surface permanent magnet machines as well. Also, the stability & reliability of these proposed motors are yet to be tested, which can only be really tested through a hardware prototype built to the specifications proposed by the optimization tool.

A possible plan to collectively address these challenges would be via a dedicated hardware prototype designed using a suitable candidate selected from the design exploration study. The prototype motor would be designed for operating at the mechanical, electrical and thermal limits, and advanced controllers and integrated power electronics would be used to keep the mo-

tor stable and reliable in its desired modes of operation. The end goal is to achieve a 2-3x increase in the motor-drive power density and similar reductions in losses compared to the current state-of-the-art.

REFERENCES

- [1] R. DelRosario, “A future with hybrid electric propulsion systems: A nasa perspective,” in *Turbine Engine Technology Symposium*, no. GRC-E-DAA-TN17600, 2014.
- [2] X. Yi, A. Yoon, and K. S. Haran, “Multi-physics optimization for high-frequency air-core permanent-magnet motor of aircraft application,” in *2017 IEEE International Electric Machines and Drives Conference (IEMDC)*. IEEE, 2017, pp. 1–8.
- [3] X. Zhang, C. L. Bowman, T. C. O’Connell, and K. S. Haran, “Large electric machines for aircraft electric propulsion,” *IET Electric Power Applications*, vol. 12, no. 6, pp. 767–779, 2018.
- [4] P. Wheeler, T. S. Sirimanna, S. Bozhko, and K. S. Haran, “Electric/hybrid-electric aircraft propulsion systems,” *Proceedings of the IEEE*, vol. 109, no. 6, pp. 1115–1127, 2021.
- [5] A. D. Anderson, N. J. Renner, Y. Wang, S. Agrawal, S. Sirimanna, D. Lee, A. Banerjee, K. Haran, M. J. Starr, and J. L. Felder, “System weight comparison of electric machine topologies for electric aircraft propulsion,” in *2018 AIAA/IEEE Electric Aircraft Technologies Symposium (EATS)*. IEEE, 2018, pp. 1–16.
- [6] A. Yoon, X. Yi, J. Martin, Y. Chen, and K. Haran, “A high-speed, high-frequency, air-core pm machine for aircraft application,” in *2016 IEEE Power and Energy Conference at Illinois (PECI)*. IEEE, 2016, pp. 1–4.
- [7] S. Huang, J. Luo, F. Leonardi, and T. A. Lipo, “A general approach to sizing and power density equations for comparison of electrical machines,” *IEEE Transactions on Industry Applications*, vol. 34, no. 1, pp. 92–97, 1998.
- [8] V. Honsinger, “Sizing equations for electrical machinery,” *IEEE transactions on energy conversion*, no. 1, pp. 116–121, 1987.
- [9] W. Soong, “Sizing of electrical machines,” *Power Engineering Briefing Note Series*, vol. 9, pp. 17–18, 2008.

- [10] “The futprint50 project,” <https://futprint50.eu/>, accessed: 2023-04-30.
- [11] X. Zhang and K. S. Haran, “High-specific-power electric machines for electrified transportation applications-technology options,” in *2016 IEEE Energy Conversion Congress and Exposition (ECCE)*. IEEE, 2016, pp. 1–8.
- [12] Z. Xia, Z. Zhu, and D. Howe, “Analytical magnetic field analysis of halbach magnetized permanent-magnet machines,” *IEEE Transactions on magnetics*, vol. 40, no. 4, pp. 1864–1872, 2004.
- [13] X. Tang and C. R. Sullivan, “Optimization of stranded-wire windings and comparison with litz wire on the basis of cost and loss,” in *2004 IEEE 35th Annual Power Electronics Specialists Conference (IEEE Cat. No. 04CH37551)*, vol. 2. IEEE, 2004, pp. 854–860.
- [14] J. Reinert, A. Brockmeyer, and R. W. De Doncker, “Calculation of losses in ferro-and ferrimagnetic materials based on the modified steinmetz equation,” *IEEE Transactions on Industry applications*, vol. 37, no. 4, pp. 1055–1061, 2001.
- [15] D. M. Ionel, M. Popescu, M. I. McGilp, T. Miller, S. J. Dellinger, and R. J. Heideman, “Computation of core losses in electrical machines using improved models for laminated steel,” *IEEE Transactions on Industry Applications*, vol. 43, no. 6, pp. 1554–1564, 2007.
- [16] “Granta materials data for simulation.” [Online]. Available: <https://www.ansys.com/products/materials/materials-data-for-simulation>
- [17] P. R. Childs, *Rotating flow*. Elsevier, 2010.
- [18] J. Veres, “Axial and centrifugal compressor mean line flow analysis method,” in *47th AIAA Aerospace Sciences Meeting including The New Horizons Forum and Aerospace Exposition*, 2009, p. 1641.
- [19] X. Yi, R. Sanchez, K. Haran, J. Veres, A. T. Perry, and P. J. Ansell, “Self-pumped air-cooling design for a high-speed high-specific-power motor,” in *2018 IEEE Transportation Electrification Conference and Expo (ITEC)*. IEEE, 2018, pp. 274–279.
- [20] P. C. Vratny, H. Kuhn, and M. Hornung, “Influences of voltage variations on electric power architectures for hybrid electric aircraft,” *CEAS Aeronautical Journal*, vol. 8, pp. 31–43, 2017.
- [21] X. Zhang, K. S. Haran, and J. Xiao, “Analytical calculation of equivalent circuit parameters and operational inductance in multiple-pole slotless pmsms,” in *2022 IEEE Transportation Electrification Conference & Expo (ITEC)*. IEEE, 2022, pp. 414–420.

- [22] Y. Wang, X. Yi, Y. Wang, X. Zhang, Y. Yin, T. Han, and K. S. Haran, “Partial discharge investigation of form-wound electric machine winding for electric aircraft propulsion,” *IEEE Transactions on Transportation Electrification*, vol. 7, no. 1, pp. 78–90, 2021.
- [23] T. Balachandran, S. Lin, C. Ward, and K. S. Haran, “Improving the thermal conductivity of form-wound litz-wire windings for slot-less machines,” in *2021 IEEE International Electric Machines & Drives Conference (IEMDC)*. IEEE, 2021, pp. 1–8.
- [24] N. Simpson, R. Wrobel, and P. H. Mellor, “Estimation of equivalent thermal parameters of impregnated electrical windings,” *IEEE Transactions on Industry Applications*, vol. 49, no. 6, pp. 2505–2515, 2013.
- [25] X. Yi, “Electromagnetic-thermal modeling for high-frequency air-core permanent magnet motor of aircraft application,” M.S. thesis, University of Illinois at Urbana-Champaign, 2016.
- [26] “Convective heat transfer coefficients table chart,” https://www.engineersedge.com/heat_transfer/convective_heat_transfer_coefficients_13378.htm, accessed: 2023-04-30.
- [27] D. A. Staton and A. Cavagnino, “Convection heat transfer and flow calculations suitable for electric machines thermal models,” *IEEE transactions on industrial electronics*, vol. 55, no. 10, pp. 3509–3516, 2008.
- [28] R. Sanchez, A. Yoon, X. Yi, L. Zheng, Y. Chen, K. S. Haran, A. Provenza, and J. Veres, “Mechanical validation of a high power density external cantilevered rotor,” *IEEE Transactions on Industry Applications*, vol. 54, no. 4, pp. 3208–3216, 2018.
- [29] D. Lee, T. Balachandran, S. Sirimanna, N. Salk, A. Yoon, P. Xiao, J. Macks, Y. Yu, S. Lin, J. Schuh et al., “Detailed design and prototyping of a high power density slotless pmsm,” *IEEE Transactions on Industry Applications*, 2022.
- [30] G. V. Brown, A. F. Kascak, B. Ebihara, D. Johnson, B. Choi, M. Siebert, and C. Buccieri, “Nasa glenn research center program in high power density motors for aeropropulsion,” National Aeronautics and Space Administration Cleveland, Tech. Rep., 2005.
- [31] P. Lolis, “Development of a preliminary weight estimation method for advanced turbofan engines,” 2014.
- [32] K. J. Yost, L. M. Chen, Z. Adamson, T. Baudendistel, W. Perdikakis, C. Kitzmiller, and J. Zhang, “Low-cost analysis methods of automotive electric machines for aviation applications,” in *2021 AIAA/IEEE Electric Aircraft Technologies Symposium (EATS)*, 2021, pp. 1–13.

- [33] S. D. Sudhoff, *Power magnetic devices: a multi-objective design approach*. John Wiley & Sons, 2021.
- [34] A. Yoon, “High-frequency, high-pole count design for improving specific power density of electric machines,” M.S. thesis, University of Illinois at Urbana-Champaign, 2016.
- [35] R. Jansen, Y. De Jesus-Arce, P. Kascak, R. W. Dyson, A. Woodworth, J. J. Scheidler, R. Edwards, E. J. Stalcup, J. Wilhite, K. P. Duffy et al., “High efficiency megawatt motor conceptual design,” in *2018 Joint Propulsion Conference*, 2018, p. 4699.
- [36] R. Hemmati, F. Wu, and A. El-Refaie, “Survey of insulation systems in electrical machines,” in *2019 IEEE International Electric Machines & Drives Conference (IEMDC)*. IEEE, 2019, pp. 2069–2076.
- [37] S. Tungare, “Modeling and control of interior permanent magnet synchronous machines at low switching-to-fundamental frequency ratios,” M.S. thesis, University of Illinois at Urbana-Champaign, 2022.